Journal of Physics Communications

PAPER

Complex field measurement in a single pixel hybrid correlation holography

Ziyang Chen[1], Darshika Singh[1,2], Rakesh Kumar Singh[1,3] and Jixiong Pu[1]

[1] College of Information Science and Engineering, Fujian Provincial Key Laboratory of Light Propagation and Transformation, Huaqiao University, Xiamen, Fujian 361021, People's Republic of China
[2] Applied and Adaptive Optics Lab, Department of Physics, Indian Institute of Space Science and Technology (IIST), Valiamala, Trivandrum, India
[3] Department of Physics, Indian Institute of Technology (BHU), Varanasi, 221003, Uttar Pradesh, India

E-mail: krakeshsingh.phy@iitbhu.ac.in

Keywords: fourier optics, laser speckle, correlation, digital holography

OPEN ACCESS

RECEIVED
21 January 2020

REVISED
3 April 2020

ACCEPTED FOR PUBLICATION
8 April 2020

PUBLISHED
16 April 2020

Abstract

We propose a new scheme for the recovery of complex-valued objects in a single-pixel hybrid correlation holography. The idea is to generate an intensity correlation hologram from the correlation of intensity fluctuations obtained over two channels, namely an optical channel equipped with a single pixel detector and a digital channel. The scheme has a theoretical basis which is described to reconstruct the objects from a single pixel detector. An experimental arrangement is proposed and as a first step towards realizing/implementing the technique, simulation of the experimental model was carried to image three complex objects.

1. Introduction

Holography allows the recording and reconstruction of a complex field. Holography with optical recording and digital reconstruction, also known as digital holography (DH), enables simultaneous quantitative imaging of amplitude and phase. Various DH schemes have been proposed to record and reconstruct the objects [1–7]. The phase imaging is essential to examine the complex-valued object. However, when the object is obscured by the scattering medium or illuminated by a random light [8–15], recovery of the non-stochastic object through phase imaging is a challenging task. Such issues have been a matter of investigation since long, and several techniques such as adaptive optics [9], correlation optics [10], and phase conjugation [15] have been proposed.

Correlation techniques like ghost imaging and ghost diffraction have drawn significant interests [16–21]. Such techniques reconstruct the object from the correlation of the intensity fluctuations from two channels (namely, test and reference). The test arm contains the object and is equipped with a bucket detector that collects the light without any spatial resolution. The reference arm needs a space-resolving optical detection. Standard ghost imaging and ghost diffraction techniques have been applied to the amplitude object. A devised Young's interferometer is developed to reconstruct the 1D complex-valued object in the ghost diffraction [19]. Ghost diffraction imaging of pure phase objects, with intensity correlation, is also described [22–25]. A number of computational correlation techniques are proposed, such as computational ghost imaging [26, 27], single-pixel imaging [28–30]. Methods to retrieve the complex field under single pixel detection are proposed by structured mask illumination [31–33].

On the other hand, over the past few years, correlation holography (CH) has emerged as a promising approach [10, 34, 35]. The CH reconstructs the object as a distribution of two point spatial coherence. Recently, a combination of optical and computational channels is proposed for the reconstruction of the object from a single pixel detector. This is referred to as the hybrid correlation holography (HCH) [36]. The HCH provides the reconstruction of the amplitude object. In this paper, a new approach to recover the complex object within the HCH framework is proposed. A comparative study (with [35, 37]) of basic principles, through theoretical explanations and difference in experimental setups, is included.

2. Theory

Consider light fields coming from two independent sources. A complex light field at time t and longitudinal propagation distance z is represented as $E_n(u, t)$, where u is a two-dimensional position vector and $n = 1, 2$ stands for two different sources. The light at the detector plane is connected with nth source as $E_n(u, t) = \int G(u, r)E_n(r, t)dr$, where r is position vector at the source plane and $G(u, r)$ represents the Fresnel propagation kernel

$$G(u, r) \approx \frac{\exp(ikz)}{i\lambda z} \exp\left(ik\frac{|u|^2 + |r|^2 - 2r \cdot u}{2z}\right)$$

where $k = 2\pi/\lambda$ is wave number and λ is wavelength of the light.

The complex field at the detector plane is coherent addition of the fields emanating from two independent sources, and given as

$$E(u, t) = E_1(u, t) + E_2(u, t) \tag{1}$$

Intensity is $I(u, t) = E^*(u, t)E(u, t)$, where * represents complex conjugate. For the Gaussian random field, the cross-covariance of the intensity is [9, 37]

$$\langle \Delta I(u)\, \Delta I(u + \Delta u)\rangle = |E_1^*(u)E_1(u + \Delta u) + E_2^*(u)E_2(u + \Delta u)|^2 = |W_1(\Delta u) + W_2(\Delta u)|^2 \tag{2}$$

where angular bracket $\langle\cdot\rangle$ denotes the ensemble average. Term $\Delta I(u) = I(u) - \langle I(u)\rangle$ is fluctuation of the intensity with respect to its mean value and $W_n(\Delta u)$ represents a two-point complex coherence function. Time t is omitted for further consideration due to monochromatic nature of the light. Due to independence of the sources, we consider $\langle E_1^*(u)E_2(u + \Delta u) = 0\rangle$ in the derivation of equation (2). Moreover, a common phase curvature of the Fresnel kernel is cancelled out in the intensity correlation, and equation (2) can be transformed to a lens-less Fourier transform hologram for the coherence waves at an arbitrary plane z [37]. The complex coherence in equation (2) takes the following form with the normalized coordinate $\Delta u \equiv \Delta u/\lambda z$

$$W_n(\Delta u) = \langle E_n^*(u)\, E_n(u + \Delta u)\rangle = \int I_n(r) \exp[-j2\pi\, r \cdot \Delta u]\, dr \tag{3}$$

where $I_n(r) = |T_n(r)|^2$ represents the incoherent source structure and $T_n(r)$ is a complex transmittance function (transparency). Only a modulus part of the transparency is involved in shaping the spatial coherence in equation (3). Using this relation, we generate a reference coherence $W_1(\Delta u)$ by an off-axis source. This provides a constant reference wave covering support of the $W_2(\Delta u)$ to record an off-axis hologram of the coherence waves. Therefore, the $W_2(\Delta u)$ can be recovered from other redundant factors in equation (2) by the Fourier analysis [37].

The experimental setup for the off-axis holography with the coherence waves is shown in figure 1(a). A monochromatic light coming out of the laser is collimated by lenses L_1, L_2 and a pinhole aperture (D) combination. This collimated beam splits into two arms by a beam splitter (BS1) and propagates through two rotating ground glass (RGG). The transmitted light from the BS1 is focused by a microscope objective (MO) at an off-axis position of the diffuser RGG1. The random field emanating from this source is represented as $E_1(r) = T_1(r)\exp[i\phi_1(r)]$, where $T_1(r)$ is source size at the RGG1 and $\phi_1(r)$ is random phase introduced by the RGG1. The off-axis position of the light at the RGG1 is controlled by steering mirror M1. The field reflected by the BS1 illuminates the transparency T and travels through RGG2. The complex amplitude of the random light immediately after the transparency is represented by $E_2(r) = T_2(r)\exp[i\phi_2(r)]$. The grain size of the random field at the transparency plane is considered to be finer than the spatial structure of the transparency. Spatial resolution is limited by the cap imposed on the spatial finesse of the transparency by the finite correlation length of the illuminating random field [35]. The random fields from the two arms of the interferometer are combined using a beam splitter BS_2 and the intensity is detected by a charged coupled device (CCD).

In contrast to application of the RGG, the proposed method based on the HCH uses a computer controlled spatial light modulator (SLM) to introduce random phases in the coherent beam and a single pixel detector rather than the CCD is used for detection of the intensity in the optical channel. Configuration of the light propagation in the optical channel in figure 1(b) is as follows. A collimated monochromatic laser beam enters into a beam displacer (BD) which splits the light into two parallel propagating orthogonally polarized components. These components propagate towards a spatial light modulator (SLM) after passing through a beam splitter (BS1). The SLM modifies only one of the orthogonally polarized components. Therefore, one of the components is flipped before and after reflection from the SLM by a half wave plate (HWP1). The SLM introduces a sequence of the random patterns into the spatially separated coherent beams, which are further folded and directed by BS1 towards a Mach–Zehnder interferometer (MZI). The random field entering into the MZI is separated into the orthogonally polarized components by a polarization beam splitter (PBS). A random field reflected from the PBS and folded by mirror M1 illuminates the transparency (T). Subsequently, this field

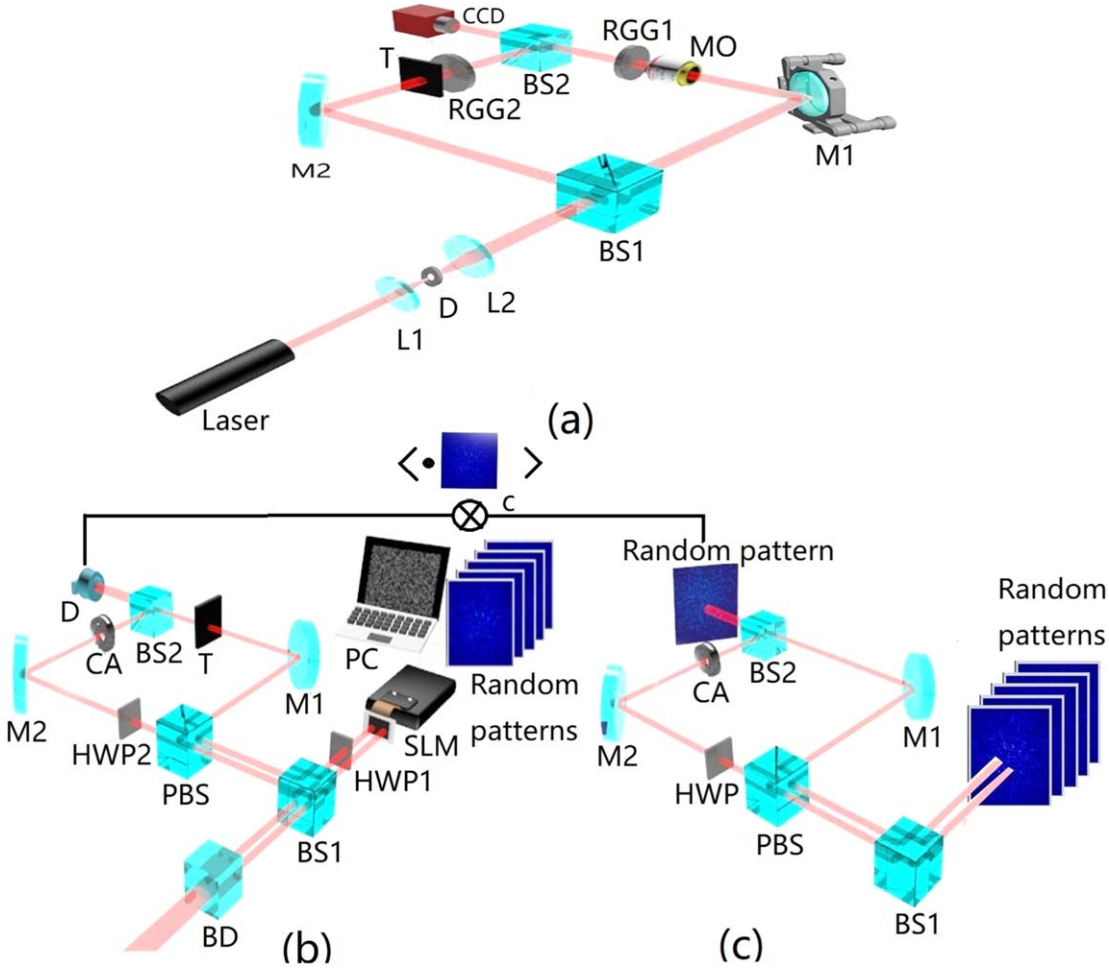

Figure 1. (a) Represents coherence waves interference setup with correlation of the intensity detected by a CCD: L-Lens, D-pin hole, BS- beam splitter, M- mirrors, T- Transparency, MO- microscope objective, RGG-rotating ground glass; (b) Optical channel in the HCH with a single pixel detector: BD- Beam Displacer, PBS-Polarization beam splitter, SLM- spatial light modulator, CA- Circular Aperture, c- correlator, D- single pixel detector (c) Architecture for digital propagation of the random fields and correlation of single point intensity with two dimensional propagated intensity.

propagates towards a single pixel detector through the BS2. On the other hand, HWP2 is used to rotate the orthogonally polarized random field passing through the PBS in order to maintain the same polarization states as in the other arm of the MZI. This field is folded by a mirror M2, and filtered by a pinhole transparency CA. The coherent random fields from the two arms of the MZI are combined using BS2 and detected by the single pixel detector D. Path lengths of the two arms of the MZI are the same. A digital channel to represent digital propagation of the random fields is shown in figure 1(c). The random light patterns introduced by the SLM are digitally propagated according to the configuration of two arms of figure 1(c). The digitally propagated random fields are interfered to generate two-dimensional random intensity patterns at the exit of BS_2 as shown in figure 1(c). The random intensity pattern from figure 1(c) is correlated with intensity measured by a single point detector as represented by the symbol (X).

The instantaneous intensity in the optical channel of figure 1(b) is represented as

$$I_o(u) = |E_o(u)|^2 = |E_o^1(u) + E_o^2(u)|^2 \tag{4}$$

where $E_o(u)$ is a complex field. The complex field and its instantaneous intensity for the digital channel are $E_c(u) = E_c^1(u) + E_c^2(u)$ and $I_c(u) = |E_c(u)|^2$, respectively.

Considering independent random fields in two arms of the MZI, the coherence function is expressed as

$$\langle E_c^*(u_1) E_o(u_2)\rangle = \langle E_c^{1*}(u_1)\, E_o^1(u_2)\rangle + \langle E_c^{2*}(u_1)\, E_o^2(u_2)\rangle \tag{5}$$

where $\langle E_c^{n*}(u_1) E_o^n(u_2)\rangle = W_{co}^n(u_1,\, u_2)$ is a complex coherence and $n = 1, 2$ represents two arms of the MZI.

Considering $u_2 = 0$ for a single pixel detector, the cross-covariance of the intensity becomes

$$\langle \Delta I_c(u)\, \Delta I_o(0)\rangle = |W_{co}^1(u) + W_{co}^2(u)|^2 \tag{6}$$

where $\Delta I_c(u)$ and $\Delta I_o(0)$ are the intensity fluctuations in the digital and the optical channels, respectively.

Consider the complex field immediately behind the transparency as $E_o^n(r) = T_n(r)\exp[j\phi^n(r)]$, where $T_n(r)$ is transparency and $\phi^n(r)$ is the random phase introduced by the SLM in nth arm of the MZI. Considering the incoherent illumination $\langle \exp[j(\phi^n(r_2) - \phi^n(r_1))]\rangle = \delta(r_2 - r_1)$, r_1 and r_2 are position vectors at the source plane. The complex coherence function in equation (6) takes the following form in the normalized coordinate $u \equiv u/\lambda z$

$$W_{co}^n(u) = \int T_n(r)\exp(-j\,2\pi\,u\cdot r)\,dr \tag{7}$$

Here transmittance function may take real or complex values. Therefore, equation (7) is influenced by amplitude and phase of the transmittance function in contrast to equation (3). To apply the holography principle in equation (6), we consider a reference coherence function as $W_{co}^1(u) = F\left\{circ\left(\frac{r-r_g}{a}\right)\right\}$. Here, F represents the Fourier transform and 'a' is the size of a circular source aperture. The circular aperture source 'a' is considered to be very small to generate a uniform reference coherence function.

This section describes the implementation of the proposed experimental model. An SLM introduces independent random phase patterns at two spatially separated locations in the incoming laser beam, as shown earlier in figure 1(b). The instantaneous random phases are represented by $\phi_{lm}^n(M)$ on lm pixel, where M represents the number of random patterns. The random fields are independent and considered to follow $\langle \exp(j\phi_{lm}^n(M))\rangle = 0$ and $\langle \exp[j(\phi_{lm}^n(M_2) - \phi_{pk}^n(M_1))]\rangle = \delta_{pl}\delta_{km}$.

A coherent beam loaded with $e^{j\phi_{nm}^1}$ propagates into a path through the pinhole CA. A coherent beam loaded with $e^{j\phi_{nm}^2}$ illuminates the transparency. Propagation effects from SLM to transparency and the pinhole are ignored. Instantaneous intensity at a single-pixel detector is represented by $I_o^\nu(0)$. Here, ν represents a random phase mask displayed on the SLM which ranges from 1 to M. The random field is also digitally propagated as shown in figure 1(c) and the instantaneous intensity $I_o^\nu(u)$ corresponding to each random mask is evaluated. The cross-covariance of the intensity is

$$\langle \Delta I_c(u)\Delta I_o(0)\rangle = \sum_{\nu=1}^{M} \Delta I_c^\nu(u)\Delta I_o^\nu(0) \tag{8}$$

here, M represents the number of random masks displayed over SLM. In each realization, random phase mask of size 300×300 is considered. The random fields in both arms of MZI are statistically independent, i.e. $\langle \exp[j(\phi_{nm}^1(M) - \phi_{nm}^2(M))]\rangle \approx 0$.

In the proposed scheme, we measure the cross-covariance of the intensities coming from two channels, namely optical and digital as explained in equation (6). An interference fringe in the intensity correlation is obtained from the correlation of the intensity fluctuations over the optical and digital channels.

3. Results

The cross-covariance and recovered complex-valued objects are shown in figure 2 for three different cases. Figure 2(a) represents the cross covariance for a digital off-axis hologram used as a transparency $T_2(r) = |O + R|^2$ in the path of random light as shown in figure 1(b). This digital off-axis hologram is a conventional hologram due to interference of the complex object O and reference R. Here the object is numeric 1. Formation of the fringe in the cross-covariance confirms coherence waves interference similar to the interference of the optical fields. A two-dimensional Fourier transform of the cross-covariance generates three spectra: the desired spectra, its conjugate and a non-modulating dc term, all separated in the frequency space depending on the off-axis position of the reference coherence. The unwanted dc spectrum can be digitally suppressed. We use either of the off-axis spectrums and translate it towards the origin of the frequency axis. The inverse Fourier transform of the filtered spectrum provides the reconstruction of complex object encoded into the digital hologram $T_2(r)$. Distribution of $W_{co}^2(u)$ shows complex object '1' and this can be explained using equation (7). Figures 2(b) and (c) show the amplitude and phase distributions of the reconstructed number '1' encoded into the off-axis hologram transparency. The strong central frequency content in figure 2(b), (as in the case of reconstruction of the off-axis hologram) is suppressed to highlight the object. The white circle in figure 2(c) highlights the phase structure of the object and its conjugate. The magnified and smoothened portion of the result is shown in the corner of each figure. This is obtained by applying the 2D Fourier Transform and interpolation of pixels in the signal domain.

In the second case, a spiral phase plate is used as phase transparency, which introduces a vortex phase structure. The light coming out of the spiral phase plate is represented as $r^m e^{im\phi}$, where r and ϕ are transverse position and azimuthal coordinates respectively and m is the topological charge of the vortex. For unit topological charge, the cross-covariance and reconstructed complex coherence are shown in figures 2(d)–(f). The presence of a fork structure in the cross-covariance in figure 2(d) confirms the existence of a vortex structure

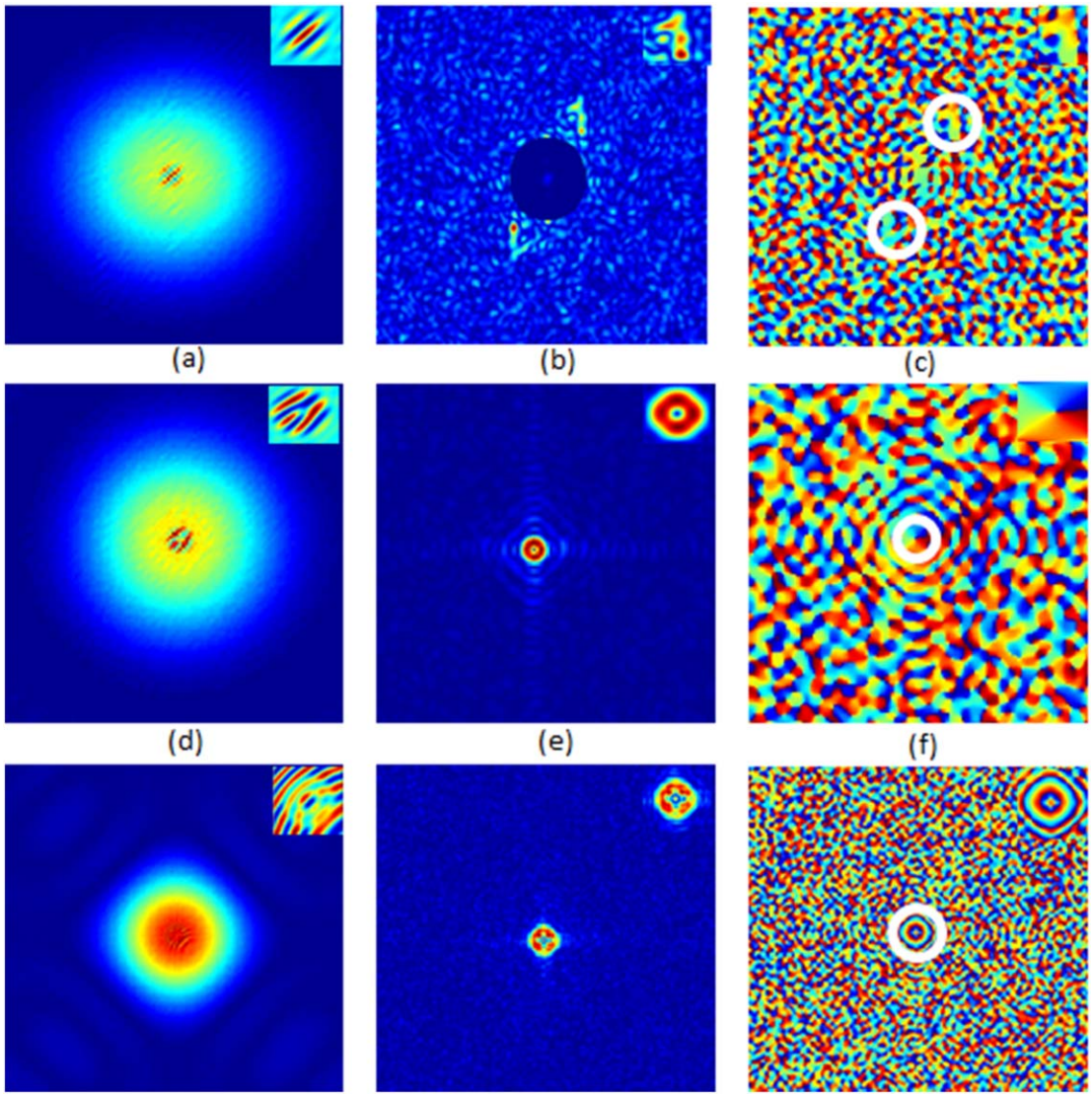

Figure 2. Recovery of the complex field in the single pixel HCH for three different transparencies: An off-axis hologram used as a transparency (a) cross-covariance of the intensity (b) amplitude of the object (c) phase of the object; A spiral phase plate as a transparency (d) cross-covariance of the intensity (e) vortex amplitude (f) vortex phase; An aperture quadratic phase as transparency (g) cross-covariance of the intensity (h) amplitude (i) phase. Interpolated portion of the results are shown in corner of each figure.

Table 1. Visibility (V) and reconstruction efficiency (R).

M = 5000	M = 30000	M = 60000	M = 100000
V = 1.77	V = 3.4	V = 5.29	V = 7.08
R = 0.639	R = 0.773	R = 0.841	R = 0.8763

in the transparency. An accumulated phase variation around the heart of the vortex core, marked by a white circle, confirms 2π phase and unit topological charge. Figures 2(g)–(i) show results for the quadratic phase mask as a transparency. The reconstruction results in figure 2 are obtained for M = 100000. The reconstruction quality depends on the transparency aperture size and M values [36]. Three different transparencies are used to highlight differences between complex coherence recovery in equations (3) and (7). For instance, recovery of vortex and quadratic phase is not possible with equation (3), whereas equation (7) preserves the signature of the complex transparency.

In order to examine the effect of M on the reconstruction quality, we evaluate reconstruction efficiency and visibility for varying M, the results are given in table 1. The visibility (V) is defined as the extent to which the reconstruction is distinguishable from the background noise. It is measured as the ratio of the average image intensity level in the region corresponding to the signal area to the average background intensity level. The

reconstruction efficiency (R) is defined as the ratio of the measured power in the signal region of the image to the sum of this and the measured power in the background region [38]. The reconstruction quality improves with an increase in the value of M.

4. Conclusions

As a conclusion, a new technique based on the interference of the coherence functions (rather than the complex fields) and utilizing the two-point intensity correlation in single pixel detection scheme is presented. This technique helps to image and reconstruct the complex field from random field illumination. The experimental geometry and results of the simulated experimental models are presented for three different cases of the transparencies. The proposed technique is expected to be useful in recovering the complex field in a single pixel hybrid correlation holography. It may also find applications in fields like high resolution imaging, polarimetry and encryption.

Acknowledgments

Science Engineering Research Board (SERB) India Grant No EMR 2015/001613, National Natural Science Foundation of China (NSFC) under grant numbers 11674111, 61575070, 11750110426; Fujian Province Science Funds for Distinguished Young Scholar 2018J06017.

ORCID iDs

Ziyang Chen https://orcid.org/0000-0002-2467-8372
Rakesh Kumar Singh https://orcid.org/0000-0002-3117-2695
Jixiong Pu https://orcid.org/0000-0001-8781-6683

References

[1] Schnars U and Jueptner W 2005 *Digital Holography* (Berlin: Springer)
[2] Poon T C 2006 *Digital Holography and Three-Dimensional Display* (Berlin: Springer)
[3] Shaked N T, Katz B and Rosen J 2009 *Appl. Opt.* **48** H121–36
[4] Micó V and Zalevsky Z 2010 *J. Biomed. Opt.* **15** 046027
[5] Osten W, Faridian A, Gao P, Körner K, Naik D, Pedrini G, Singh A K, Takeda M and Wilke M 2014 *Appl. Opt.* **53** G44
[6] Shtraikh E, Zieder M, Kelner R and Rosen J 2015 *Asian J. of Physics* **24** 1659–66
[7] Tahara T, Quan X, Otani R, Takaki Y and Matoba O 2018 *Microscopy* **67** 55–67
[8] Tyson R K 2010 *Principles of Adaptive Optics* (New York: Academic)
[9] Goodman J 2007 *Speckle Phenomena in Optics: Theory and Applications* (Roberts and Company)
[10] Takeda M, Wang W, Naik D N and Singh R K 2014 *Opt. Rev.* **21** 849–61
[11] Katz O, Heidmann P, Fink P and Gigan S 2014 *Nature Photon.* **8** 784–90
[12] Singh A K, Naik D N, Pedrini G, Takeda M and Osten W 2017 *Light Sci. Appl.* **6** e16219
[13] Mukherjee S, Vijayamumar A, Kumar M and Rosen J 2018 *Sci. Rep.* **8** 1134
[14] Okamoto Y, Horisaki R and Tanida J 2019 *Opt. Lett.* **44** 2526–9
[15] Shin S, Lee K R, Baek Y S and Park Y K 2018 *Phys. Rev. Appl.* **9** 044042
[16] Gatti A, Brambilla E, Bache M and Lugiato L A 2004 *Phys. Rev. Lett.* **93** 093602
[17] Cai Y and Zhu S Y 2005 *Phys. Rev. E* **71** 056607
[18] Ferri F, Magatti D, Gatti A, Bache M, Brambilla E and Lugiato L A 2005 *Phys. Rev. Lett.* **94** 183602
[19] Borghi R, Gori F and Santarsiero M 2006 *Phys. Rev. Lett.* **96** 183901
[20] Zhang S H, Gao L, Xiong J, Feng L J, Cao D Z and Wang K 2009 *Phys. Rev. Lett.* **102** 073904
[21] Bache M, Magatti D, Ferri F, Gatti A, Brambilla E and Lugiato L A 2006 *Phys. Rev. A* **73** 053802
[22] Ishikawa K, Takahashi E and Midorikawa K 2007 *Phys. Rev. A* **75** 021801(R)
[23] Gong W and Han S 2010 *Phys. Rev. A* **82** 023828
[24] Shirai T, Setälä T and Friberg A T 2011 *Phys. Rev. A* **84** 041801(R)
[25] Zhang D J, Tang Q, Wu T F, Qiu H C, Xu D Q, Li H G, Wang H B, Xiong J and Wang K 2014 *Appl. Phys. Lett.* **104** 121113
[26] Shapiro J H 2008 *Phys. Rev. A* **78** 061802(R)
[27] Bromberg Y, Katz O and Silberberg Y 2009 *Phys. Rev. A* **79** 053840
[28] Sun B, Edgar M P, Bowman R, Vittert L E, Welsh S, Bowman A and Padgett M J 2013 *Science* **340** 844
[29] Clemente P, Duran V, Tajahuerce E, Torres-Company V and Lancis J 2012 *Phys. Rev. A* **86** 041803(R)
[30] Zhang Z, Wang X, Zheng G and Zhong J 2017 *Opt. Express* **25** 19619–39
[31] Zhang Z and Zhong J 2016 *Opt. Lett.* **41** 2497–500
[32] Martinez-Leon L, Clemente P, Mori Y, Climent V, Lancis J and Tajahuerce E 2017 *Opt. Express* **25** 4975–84
[33] Ota K and Hayasaki Y 2018 *Opt. Lett.* **43** 3682–5
[34] Naik D N, Singh R K, Ezawa T, Miyamoto Y and Takeda M 2011 *Opt. Express* **19** 1408–21
[35] Singh R K, Vinu R V and Sharma A M 2014 *Appl. Phys. Lett.* **104** 111108
[36] Singh R K 2017 *Opt. Lett.* **42** 2515–8
[37] Singh R K, Vyas S and Miyamoto Y 2017 *J. Opt.* **19** 115705
[38] Hillman T R, Yamauchi T, Choi W, Dasari R R, Feld M S, Park Y K and Yaqoob Z 2013 *Scient. Rep.* **3** 1909